

# $f_0(1370)$

D.V. Bugg<sup>1</sup>,

Queen Mary, University of London, London E1 4NS, UK

## Abstract

A summary is given of the main sets of data requiring the existence of  $f_0(1370)$ . Crystal Barrel data on  $\bar{p}p \rightarrow \eta\eta\pi^0$  contain a visible  $f_0(1370)$  peak and require at least a  $19\sigma$  contribution. This alone is sufficient to demonstrate its existence. More extensive data on  $\bar{p}p \rightarrow 3\pi^0$  at rest contain delicate interferences which determine the mass and width independently in  $^1S_0$  and  $^3P_1$  annihilation and agree within 5 MeV for both mass and width. The peak in  $2\pi$  is at  $1282 \pm 5$  MeV, but the rapid increase in  $4\pi$  phase space with mass displaces the  $4\pi$  peak to 1360 MeV. BES II data for  $J/\Psi \rightarrow \phi\pi^+\pi^-$  contain a visible  $f_0(1370) \rightarrow 2\pi$  signal  $> 8\sigma$ . In all cases, a resonant phase variation is required.

PACS: 13.25.Gv, 14.40.Gx, 13.40.Hq

The  $f_0(1370)$  plays a vital role in the spectroscopy of light  $J^P = 0^+$  mesons. Several authors have questioned its existence, though these criticisms are based on fits to very limited sets of data. To answer those questions, the best available data have been refitted critically. Full details of the analysis are given in [1]. Here essential points are summarised.

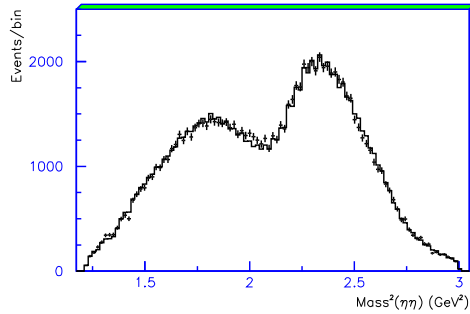


Figure 1: The  $\eta\eta$  mass projection for  $\bar{p}p \rightarrow \eta\eta\pi^0$  at rest in liquid hydrogen

Crystal Barrel data on  $\bar{p}p \rightarrow (\eta\eta)\pi^0$  at rest in liquid and gaseous hydrogen show two clear peaks in  $\eta\eta$  at  $\sim 1330$  and  $1500$  MeV [2], see Fig. 1. The low mass peak cannot be due to  $f_2(1270)$ , whose branching ratio to  $\eta\eta$  is very small. A fit without  $f_0(1370)$  is worse by 19 standard deviations, because the peak at 1330 and the dip at 1430 MeV cannot be fitted by  $\sigma \rightarrow 4\pi$  and  $a_0(980)$  alone. These data alone are sufficient to demonstrate the existence of  $f_0(1370)$ .

The data which determine resonance parameters best are Crystal Barrel data on  $\bar{p}p \rightarrow 3\pi^0$  at rest in liquid and gaseous hydrogen [3]. There is a conspicuous signal at low mass due to the  $\sigma$  pole and high mass peaks due to  $f_2(1270)$  and  $f_0(1500)$ . The  $f_0(1370)$  hides beneath the  $f_2(1270)$ , but is clearly separated by angular analysis. Interferences between the three  $\pi\pi$  combinations determine the mass and width of  $f_0(1370)$  in a very delicate way. The two sets of data allow a clean separation of annihilation from  $^1S_0$  and  $^3P_1$  initial states. The  $f_0(1370)$  is at least a 32 standard deviation signal in  $^3S_1$  and 33 standard deviations in  $^3P_1$ .

The opening of the  $4\pi$  channel plays an important role. The phase space for  $\rho\rho$  and  $\sigma\sigma$  are shown in Fig. 2. Relative contributions are poorly known, so the fit to data finds the best compromise: a Fermi function going to 1 at high mass. Half-height is at  $\sim 1.8$  GeV, and  $4\pi$  inelasticity is small at 1.3 GeV, ultimately the best mass.

The full form of the Breit-Wigner resonance formula,

$$f = 1/[M^2 - s - m(s) - iM\Gamma_{total}(s)] \quad (1)$$

contains a real dispersive term  $m(s)$  [4], which for the  $4\pi$  channel reads

$$m(s) = \frac{s - M^2}{\pi} \int \frac{ds' M\Gamma_{4\pi}(s')}{(s' - s)(s' - M^2)}. \quad (2)$$

<sup>1</sup>email address: D.Bugg@rl.ac.uk

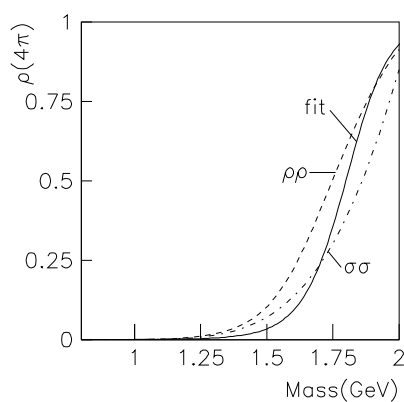


Figure 2:  $4\pi$  phase space for  $\rho\rho$  (dashed),  $\sigma\sigma$  (chain curve) and the fit adopted here (full curve)

The slope of  $m(s)$  near resonance is larger than  $(M^2 - s)$ . This point was not realised in earlier work. Nevertheless, a good solution emerges naturally. Loop diagrams for production of the  $4\pi$  system behave like vacuum polarisation and lead to strong renormalisation effects. In consequence, only the ratio of  $2\pi$  and  $4\pi$  widths is well determined: the absolute values can be varied through a wide range, leaving the line-shape almost unchanged.

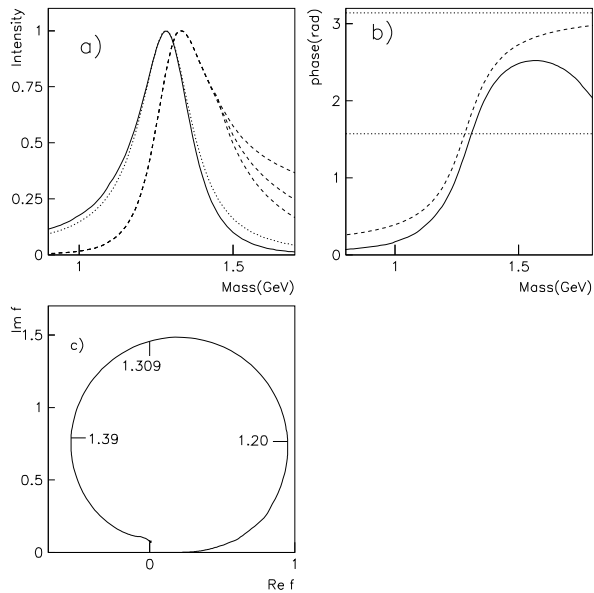


Figure 3: (a) line-shapes of  $f_0(1370)$  for  $2\pi$  (full curve), a Breit-Wigner amplitude with constant width (dotted), and for  $4\pi$  (dashed); (b) the phase angle measured from the bottom of the Argand plot (full curve) and for a Breit-Wigner amplitude of constant width (dashed); horizontal lines mark phase shifts of  $\pi/2$  and  $\pi$ , (c) Argand plot; masses are shown in GeV.

Fig. 3 shows the essential points. The  $\pi\pi$  peak is at  $1282 \pm 5$  MeV and is cut off towards higher masses by the opening of the  $4\pi$  channel. The Breit-Wigner denominator is the same for  $4\pi$  data, but  $4\pi$  phase space displaces the  $4\pi$  peak upwards by  $78 \pm 10$  MeV. This explains confusion in the Particle Data tables, where the mass is quoted as 1200–1500 MeV. One must distinguish between experiments fitting (a) two-body channels and (b)  $4\pi$  data. The centre of the  $4\pi$  peak at half-height is at 1390 MeV, in close agreement with extensive Crystal Barrel fits [5]. The three dashed curves above 1500 MeV illustrate uncertainty in  $\Gamma(4\pi)$ .

A remarkable feature of the new analysis is shown in Fig. 3(c). Despite the strong dispersive effect of the  $4\pi$  channel, the amplitude follows a circle very closely. The left-hand side of the loop is suppressed by coupling to  $4\pi$ . The phase shift goes through  $90^\circ$  at  $1309 \pm 5$  MeV, but the circle can be reproduced well with an effective mass of 1282 MeV and a constant width of  $207 \pm 15$  MeV.

Fig. 4 displays the Argand diagram for the  $\pi\pi$  S-wave in  $^1S_0 \bar{p}p \rightarrow 3\pi^0$ . There are successive loops due to the  $\sigma$  pole,  $f_0(980)$ ,  $f_0(1370)$  and  $f_0(1500)$ . The third loop is the crucial one identifying  $f_0(1370)$ , or  $f_0(1300)$  to give it a new and improved mass. An important test is to fit 40 MeV bins from 1100 to 1460 MeV freely in magnitude and phase. Real and imaginary parts of the amplitude move from the fitted curve only by  $\sim 15\%$  of the radius of the loop, consistent with experimental errors. This shows that the loop is definitely required.

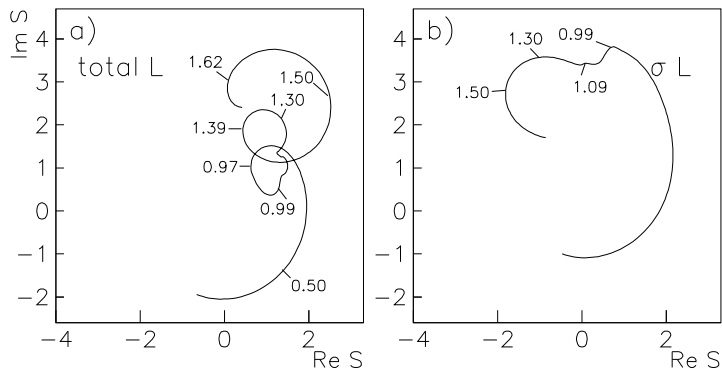


Figure 4: Argand diagrams for the total  $\pi\pi$  S-wave in liquid hydrogen and  $\sigma$  alone; masses are marked in GeV

A vital point in the new analysis is the inclusion of  $\sigma \rightarrow 4\pi$ . This cannot account for the  $f_0(1370)$  loop, as illustrated on Fig. 4(b). There is a loop near 1500 MeV due to this process, but it is higher and much wider than  $f_0(1370)$ . A weakness of all current fits to  $4\pi$  data is the omission of the  $\sigma \rightarrow 4\pi$  amplitude.

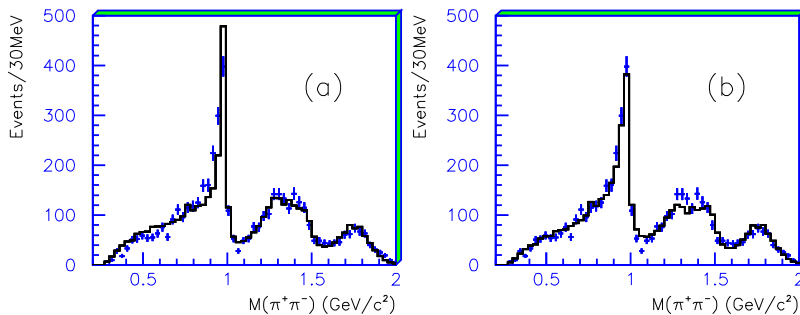


Figure 5: Fits to BES II data on  $J/\Psi \rightarrow \phi\pi^+\pi^-$ . (a) optimum fit; (b) without  $f_0(1370)$ .

The  $f_0(1370)$  and  $f_0(1500)$  combine to produce a visible peak in BES data for  $J/\Psi \rightarrow \phi\pi^+\pi^-$  [6]. That publication fitted the mass and width freely. These data have now been refitted using parameters fitted to the  $3\pi^0$  and  $\eta\eta\pi^0$  data. The fit of Fig. 5(a) is acceptable. If the  $f_0(1370)$  is removed, Fig. 5(b) shows the fit is visibly poor. Incidentally, the  $f_0(1370)$  is well separated by angular analysis from  $f_2(1270)$  in these data; the latter optimises with mass and width consistent with PDG values.

All the three sets of data discussed so far require a resonant phase variation for  $f_0(1370)$ . If the resonance is replaced with a peak of the same line-shape but no phase variation (despite the fact that this is non-analytic),  $\chi^2$  is significantly worse in every case.

The  $f_0(1370)$  also appears in GAMS data for  $\pi^+\pi^- \rightarrow \pi^0\pi^0$  at large  $|t|$  [7] and in central production of  $\pi\pi$  with parameters close to those found here [8]. Historically, it was first identified as  $\epsilon(1300)$  in data from the Argonne and Brookhaven labs on  $\pi\pi \rightarrow KK$  [9]. That identification was not clear-cut because parameters of  $f_0(980)$  and  $\sigma \rightarrow KK$  were not known accurately at that time. Using modern values for those parameters, these early data are entirely consistent with those fitted here [10].

The new fit includes the BES data for  $J/\Psi \rightarrow \omega\pi\pi$  [11] as an important constraint on the line-shape of the  $\sigma$  up to 1050 MeV; it is clearly visible by eye in the  $\pi\pi$  mass projection in those data. The  $\pi\pi$  phase shifts predicted by Caprini et al. [12] using the Roy equations are also included. The moments for Cern-Munich data on  $\pi\pi \rightarrow \pi\pi$  [13] are also refitted. Up to the  $KK$  threshold, these data determine  $\pi\pi$  phases with errors of  $\sim 3.5^\circ$ . However, above the  $KK$  threshold, real and imaginary parts of the amplitude become very strongly correlated because differential cross sections alone do not separate magnitude and phase. The fit requires inclusion of some mixing between  $\sigma$ ,  $f_0(1370)$  and  $f_0(1500)$ . The Argand diagram for the  $\pi\pi$   $I = 0$  S-wave is shown in Fig. 6. There is a loop due to  $f_0(1370)$ , crossing the Argand plot rapidly at 1230 MeV. The fit to Cern-Munich data gives  $\Gamma_{2\pi}[f_0(1500)] = 61 \pm 5$  MeV. The following branching ratios are also determined:  $\Gamma(f_0(1370) \rightarrow \eta\eta)/\Gamma(f_0(1370) \rightarrow \pi\pi) = 0.19 \pm 0.07$ ,  $\Gamma(f_0(1500) \rightarrow \eta\eta)/\Gamma(f_0(1500) \rightarrow \pi\pi) = 0.135 \pm 0.05$ ,  $\Gamma(\sigma \rightarrow \eta\eta)/\Gamma(\sigma \rightarrow \pi\pi) = 0.19 \pm 0.07$ .

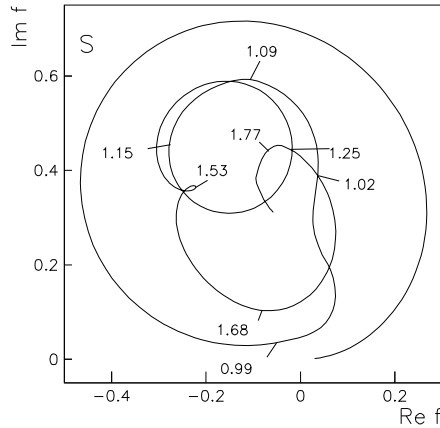


Figure 6: Argand diagram for  $\pi\pi$   $I = 0$  S-wave in elastic scattering

In summary, the  $f_0(1370)$  is definitely required and can be approximated for most purposes with a Breit-Wigner denominator with  $M = 1282 \pm 5$  MeV,  $\Gamma = 207 \pm 15$  MeV, and appropriate phase space in the numerator for each channel. Together with  $a_0(1450)$ ,  $K_0(1430)$ ,  $f_0(1710)$  and  $f_0(1500)$ , one can complete a nonet together with the  $0^+$  glueball which mixes with the  $q\bar{q}$  states. The  $f_0(1790)$  observed in BES data for  $J/\Psi \rightarrow \phi\pi\pi$  (and several other sets of data) makes the first member of the next nonet. The exotic  $\phi\omega$  peak observed by BES in  $J/\Psi \rightarrow \gamma\phi\omega$  [14] is consistent with the upper half of  $f_0(1790)$ , suggesting it is locked to this threshold at 1801 MeV, similar to the way  $f_2(1565)$  is locked to the  $\omega\omega$  threshold [15].

## References

- [1] D.V. Bugg, Eur. Phys. J C **52** 55 (2007); arXiv: hep-ex/0706.1341
- [2] C. Amsler et al., Phys. Lett. B **291** 347 (1992)
- [3] A. Abele et al., Nucl. Phys. A **609** 562 (1996)
- [4] A.V. Anisovich et al., Nucl. Phys. A **690** 567 (2001)
- [5] A. Abele et al., Eur. Phys. J. C **19** 667 (2001) and **21** 261 (2001)
- [6] M. Ablikim et al., Phys. Lett. B **607** 243 (2005)
- [7] D. Alde et al., Eur. Phys. J. A **3** 361 (1998)
- [8] D. Barberis et al., Phys. Lett. B **474** 423 (2000)
- [9] V.A. Polychronakos et al., Phys. Rev. D **19** 1317 (1979); D. Cohen et al., Phys. Rev. D **22** 2595 (1980); A.D. Martin and E.N. Ozmütlu, Nucl. Phys. B **158** 520 (1979) A. Etkin et al., Phys. Rev. D **25** 1786 (1982)
- [10] D.V. Bugg, Euro. Phys. J C **47** 45 (2006)
- [11] M. Ablikim et al., Phys. Lett. B **598** 149 (2004)
- [12] I. Caprini, I. Colangelo and H. Leutwyler, Phys. Rev. Lett. **96** 032001 (2006)
- [13] W. Ochs, University of Munich Ph.D. thesis (1974)
- [14] M. Ablikim et al., Phys. Rev. Lett. **96** 162002 (2006)
- [15] C.A. Baker et al., Phys. Lett. B **467** 147 (1999)